PHYSICAL REVIEW C **77**, 034311 (2008)

High-spin, multiparticle isomers in ^{121,123}Sb

G. A. Jones,[1,*] S. J. Williams,[1,2] P. M. Walker,[1] Zs. Podolyák,[1] S. Zhu,[3] M. P. Carpenter,[3] J. J. Carroll,[4] R. S. Chakrawarthy,[2] P. Chowdhury,[5] I. J. Cullen,[1] G. D. Dracoulis,[6] A. B. Garnsworthy,[1] G. Hackman,[2] R. V. F. Janssens,[3] T. L. Khoo,[3] F. G. Kondev,[7] G. J. Lane,[6] Z. Liu,[1] D. Seweryniak,[3] and N. J. Thompson[1]

[1]*Department of Physics, University of Surrey, Guildford GU2 7XH, United Kingdom*

[2]*TRIUMF, 4004 Westbrook Mall, Vancouver, British Columbia, V6T 2A3, Canada*

[3]*Physics Division, Argonne National Laboratory, Argonne, Illinois 60439, USA*

[4]*Department of Physics and Astronomy, Youngstown State University, Youngstown, Ohio 44555, USA*

[5]*University of Massachusetts Lowell, Lowell, Massachusetts 01854, USA*

[6]*Department of Nuclear Physics, RSPhysSE, Australian National University, Canberra 0200, Australia*

[7]*Nuclear Engineering Division, Argonne National Laboratory, Argonne, Illinois 60439, USA*

(Received 31 May 2007; published 25 March 2008)

Isomers in near-spherical $Z = 51$, antimony isotopes are reported here for the first time using fusion-fission reactions between ^{27}Al and a pulsed ^{178}Hf beam of energy, 1150 MeV. γ rays were observed from the decay of isomeric states with half-lives, $T_{1/2} = 200(30)$ and $52(3)\,\mu$s, and angular momenta $I = (\frac{25}{2})$ and $I^\pi = \frac{23}{2}^+$, in ^{121,123}Sb, respectively. These states are proposed to correspond to $\nu(h_{\frac{11}{2}})^2$ configurations, coupled to an odd $d_{\frac{5}{2}}$ or $g_{\frac{7}{2}}$ proton. Nanosecond isomers were also identified at $I^\pi = \frac{19}{2}^-$ [$T_{1/2} = 8.5(5)$ ns] in ^{121}Sb and $I^\pi = (\frac{15}{2}^-)$ [$T_{1/2} = 37(4)$ ns] in ^{123}Sb. Information on spins and parities of states in these nuclei was obtained using a combination of angular correlation and intensity-balance measurements. The configurations of states in these nuclei are discussed using a combination of spin/energy systematics and shell-model calculations for neighboring tin isotones and antimony isotopes.

DOI: 10.1103/PhysRevC.77.034311 PACS number(s): 23.20.Lv, 23.20.En, 25.70.Jj, 27.60.+j

I. INTRODUCTION

Nuclei near closed shells represent an excellent opportunity to probe important facets of nuclear structure. Nuclides close to the $Z = 50$ shell closure are particularly good for such investigations, due to the experimental accessibility of many $Z = 50$, tin nuclei across the $N = 50$–82 shell. Of recent interest in this region is the energy evolution of spherical proton orbitals with increasing neutron excess, particularly $\pi d_{\frac{5}{2}}, \pi g_{\frac{7}{2}}$, and $\pi h_{\frac{11}{2}}$ [1,2]. These effects are best explored in antimony nuclei, with one proton outside a $Z = 50$ core. One of the first indications of this orbital evolution came from the observation of a change in the ground-state quantum number for antimony nuclei, from $I^\pi = \frac{5}{2}^+$ in ^{121}Sb to $\frac{7}{2}^+$ in ^{123}Sb [3]. The energy difference between the first excited $\frac{5}{2}^+$ and $\frac{7}{2}^+$ states changes by nearly 1.5 MeV in odd-A antimony nuclei from $117 \leqslant A \leqslant 133$, interpreted as a decrease in energy of the $\pi g_{\frac{7}{2}}$ orbital relative to $\pi d_{\frac{5}{2}}$ state [1]. This change in energy difference has been interpreted as a signature for the presence of a strong tensor force [4] or a decreasing spin-orbit interaction for the $d_{\frac{5}{2}}, g_{\frac{7}{2}}$, and $h_{\frac{11}{2}}$ levels with increasing neutron excess [1,2]. These are both consistent with an empirical reduction in relative energy between the $g_{\frac{7}{2}}$ and $h_{\frac{11}{2}}$ proton orbitals, which changes by $\sim$2 MeV over odd-A antimony nuclei with $117 \leqslant A \leqslant 133$ [1,2].

Nuclei near closed-shell boundaries are also a good place to simultaneously study both collective and multiparticle excitations. Strongly coupled rotational structures, built on $\pi h_{\frac{11}{2}}$ intruder and $\pi(g_{\frac{9}{2}})^{-1}$ excitations, are observed in odd-A antimony nuclei with $113 \leqslant A \leqslant 121$ [5–8]. As the neutron number increases and the closed $N = 82$ shell is approached, however, the excitation energy of these deformed states increases, and the rotational bands are no longer yrast; the $\pi\frac{9}{2}[404]$ state becomes nonyrast in ^{123}Sb ($N = 72$), increasing in energy to $E_x = 1337$ keV [9,10]. This simplifies the picture dramatically, because all states can be interpreted as spherical single or multiparticle excitations. In particular, many states can be described in terms of those observed in tin nuclei, coupled to an extra proton [11,12]. Nevertheless, the many valance particles make it difficult to perform detailed shell-model calculations, and comprehensive experimental data provide a benchmark against which to test the development of appropriate theoretical descriptions.

This article describes the identification of states in ^{121,123}Sb from the decay of previously unreported isomeric states.

II. EXPERIMENTAL PROCEDURE

The experiment was performed at Argonne National Laboratory using the Argonne Tandem Linear Accelerator System (ATLAS), which delivered a ^{178}Hf beam onto a ^{208}Pb target at a laboratory energy of 1150 MeV, to study long-lived isomeric states in hafnium-like nuclei (presented in Ref. [13]). This article reports results obtained from incidental fusion-fission reactions between the ^{178}Hf projectiles and a ^{27}Al frame supporting the ^{208}Pb target. Fission of the ^{205}At compound nucleus populated nuclei with large yields, from $_{34}$Se to $_{54}$Xe.

*gareth.jones2@barcap.com

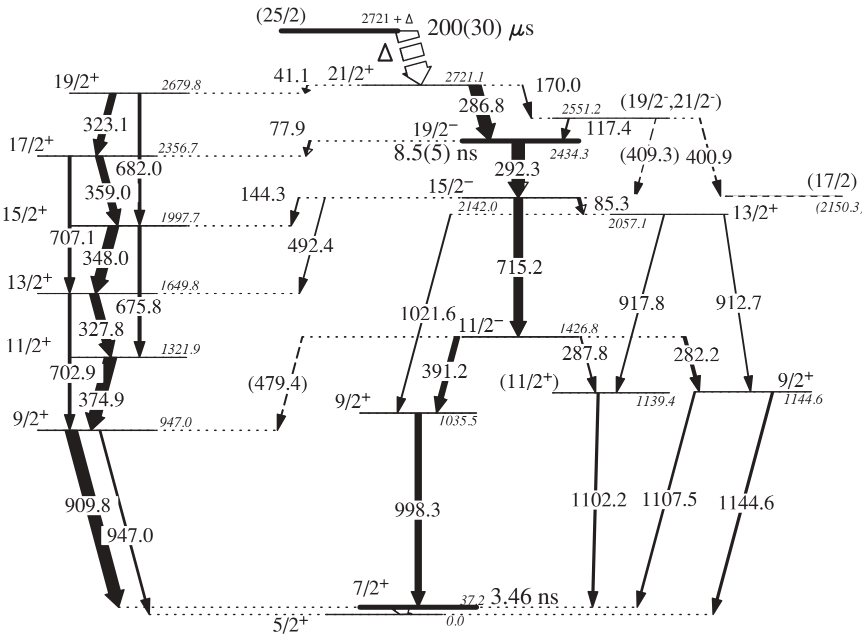

FIG. 1. Level scheme for transitions in ^{121}Sb, observed in the long-pulsing experiment from the decay of a $T_{1/2} = 200(30)\,\mu$s isomer. Widths of arrows indicate the intensity of particular γ-ray decays.

The resulting γ-ray decays from all reaction products were measured using the Gammasphere array [14], comprising 101 Compton-suppressed germanium detectors in this experiment. The beam was bunched into short pulses of width ∼0.5 ns, separated by periods of 82.5 ns. This pulsing was utilized to deliver *short* and *long* pulsed-beam conditions, enabling the study of metastable states in the $10^{-9} \rightarrow 10^{-4}$ s range. In the short-pulsing experiment, 1 of 10 beam pulses was incident on the target, resulting in a 825-ns inspection period within which delayed γ-ray decays could be studied. Events where two or more coincident γ rays were detected within a 2-μs range were written to tape for subsequent off-line analysis. In the long-pulsing measurement, a 25-μs beam-on period preceded a 75-μs beam-off period during which the data acquisition system was triggered by single γ-ray events and time stamped using an external 10-MHz oscillator clock. Great care was taken to calibrate the HPGe detectors for γ-ray energy measurements, using a number of γ-ray sources.

III. DATA ANALYSIS

The nature of the fusion-fission reaction process leads to the detection of a large number of γ rays emitted from excited states in a broad range of nuclei, resulting in a highly complex data set. Due to this level of complexity, it was necessary to utilize multidimensional γ-ray coincidence techniques to correlate decays associated with particular nuclides. A number of coincidence cubes corresponding to different γ-ray time and energy coincidence conditions were created for both the short-pulsing and long-pulsing experiments. These were analyzed with software packages described in Refs. [15–17].

A combination of the high statistics obtained in this experiment and the high granularity of the Gammasphere detector array allow for a γ-γ angular correlation analysis to be performed on pairs of coincident transitions from the decay of isomeric states. Each of the detectors in the Gammasphere array is associated with angles (θ, ϕ) with respect to the orientation of the beam axis. Pairs of γ-ray coincidence events $(E_{\gamma_1}, E_{\gamma_2})$ were placed into symmetric matrices according to the angle between the detectors, δ, expressed by $\cos\delta = \cos(\phi_2 - \phi_1) \times \sin\theta_1 \sin\theta_2 + \cos\theta_1 \cos\theta_2$ [18]. The detector pairs were grouped into 11 bins with average angular differences of $\bar{\delta} = 22^\circ, 40^\circ, 54^\circ, 66^\circ, 76^\circ, 90^\circ, 104^\circ, 114^\circ, 126^\circ, 140^\circ$, and 158°, each with $350 < N < 700$ combinations. The groups were chosen to evenly spread the number of detector combinations over a range of $\cos^2(\delta)$ values. The intensity of a given transition pair was measured for each of the groupings using the symmetric matrices, and normalized with the relative efficiency of the detector pairs. Angular-correlation coefficients (A_{kk}) were obtained from a fit to the intensities of the γ-$\gamma(\delta)$ coincidence events to the function:

$$W(\delta) = 1 + A_{22}P_2(\cos\delta) + A_{44}P_4(\cos\delta), \qquad (1)$$

where P_2 and P_4 are Legendre polynomials. Values of A_{kk} were compared with those calculated, using the procedure described in Ref. [19].

IV. RESULTS

A. ^{121}Sb

Transitions from the decay of a previously unobserved microsecond isomer were identified in the long-pulsing experiment. γ rays from the decay of states in ^{121}Sb were identified in projections of double coincidence gates placed on γ rays from Ref. [11]. The updated level scheme from the analysis of this experiment is illustrated in Fig. 1; three states at energy, $E_x = 2057.1$, 2150.3, and 2551.2 keV are reported for the first time. Table I provides a summary of all ^{121}Sb transitions observed in the measurement; asterisks (*) indicate transitions observed for the first time. The relative γ-ray intensities were established from spectra under different double-gating conditions.

TABLE I. Transitions observed in ^{121}Sb from the $T_{1/2} = 200(30)$ μs isomer in the long-pulsing experiment. Relative intensity measurements are provided for γ-ray decays in the rotational [$I_\gamma(R)$] and single-particle structures [$I_\gamma(S)$] on the left and right side of Fig. 1, respectively. The normalized ratio of the rotational to single-particle structure intensities is 0.7(1). Transitions observed for the first time are marked with asterisks (*).

E_γ (keV)	E_i (keV)	E_f (keV)	J_i^π	J_f^π	$I_\gamma(R)$	$I_\gamma(S)$
41.1(5)*	2721.1	2679.8	$21/2^+$	$19/2^+$	5.0(9)	–
77.9(3)*	2434.3	2356.7	$19/2^-$	$17/2^+$	9.4(10)	–
85.3(3)*	2142.0	2057.1	$15/2^-$	$13/2^+$	–	18(2)
117.4(3)*	2551.2	2434.3	$(21/2^-,19/2^-)$	$19/2^-$	–	2.5(3)
144.3(5)*	2142.0	1997.7	$15/2^-$	$15/2^+$	<1	<1
170.3(3)*	2721.1	2551.2	$21/2^+$	$(21/2^-,19/2^-)$	–	4.0(5)
282.2(3)	1426.8	1144.6	$11/2^-$	$9/2^+$	–	23(3)
286.8(3)	2721.1	2434.3	$21/2^+$	$19/2^-$	13.3(14)	100
287.8(4)	1426.8	1139.4	$11/2^-$	$(11/2^+)$	–	6.9(9)
292.3(3)	2434.3	2142.0	$19/2^-$	$15/2^-$	3.9(5)	98(9)
323.1(3)	2679.8	2356.7	$19/2^+$	$17/2^+$	53(5)	–
327.8(3)	1649.8	1321.9	$13/2^+$	$11/2^+$	70(7)	–
348.0(3)	1997.7	1649.8	$15/2^+$	$13/2^+$	84(9)	–
359.0(3)	2356.7	1997.7	$17/2^+$	$15/2^+$	58(6)	–
375.0(3)	1321.9	947.0	$11/2^+$	$9/2^+$	98(10)	–
391.2(3)	1426.8	1035.5	$11/2^-$	$9/2^+$	–	43(5)
400.9(4)*	(2551.2)	(2150.3)	$(21/2^-,19/2^-)$	$(17/2)$	–	5.8(7)
(409.3(6))*	2551.2	2142.0	$(21/2^-,19/2^-)$	$15/2^-$	–	1.7(4)
(479.4(4))*	1426.8	947.0	$11/2^-$	$9/2^+$	–	<1
492.4(4)*	2142.0	1649.8	$15/2^-$	$13/2^+$	3.0(4)	1.4(4)
675.8(3)	1997.7	1321.9	$15/2^+$	$11/2^+$	23(3)	–
682.0(3)	2679.8	1997.7	$19/2^+$	$15/2^+$	20(2)	–
702.9(3)	1649.8	947.0	$13/2^+$	$9/2^+$	20(2)	–
707.1(3)	2356.7	1649.8	$17/2^+$	$13/2^+$	21(2)	–
715.2(3)	2142.0	1426.8	$15/2^-$	$11/2^-$	–	72(7)
909.8(3)	947.0	37.2	$9/2^+$	$7/2^+$	100	–
912.7(4)*	2057.1	1144.6	$13/2^+$	$9/2^+$	–	3.7(5)
917.8(4)*	2057.1	1139.4	$13/2^+$	$(11/2^+)$	–	9.3(10)
947.0(4)	947.0	0.0	$9/2^+$	$5/2^+$	11.7(14)	–
998.3(4)	1035.5	37.2	$9/2^+$	$7/2^+$	–	51(5)
1021.6(5)*	2057.1	1035.5	$13/2^+$	$9/2^+$	–	5.2(7)
1102.2(5)	1139.4	37.2	$(11/2^+)$	$7/2^+$	–	15.9(17)
1107.5(3)	1144.6	37.2	$9/2^+$	$7/2^+$	–	10.8(12)
1144.6(3)	1144.6	0.0	$9/2^+$	$5/2^+$	–	15.3(17)

Two distinctly different structures are present in the level scheme of Fig. 1, linked by low-intensity transitions. The structure on the left side is the rotational band built on the $\pi\frac{9}{2}[404]$ orbital [8], also observed in lighter odd-A antimony isotopes with $113 \leqslant A \leqslant 119$ [5–8]. The spins and parities of these states are assigned accordingly. The order of states on the right side of Fig. 1 is indicative of noncollective, single, and multiparticle excitations.

Figure 2(a) provides the time projection from several γ-γ gates on transitions following the decay of the microsecond isomer. The half-life was measured to be $T_{1/2} = 200(30)$ μs. Spectra illustrating γ rays observed in the rotational and single-particle decay structures are provided in Figs. 2(b)–2(e).

The observation of the 41-keV transition [illustrated in Fig. 2(b)], which approaches the low-energy detection limit of Gammasphere, is a valuable link between the rotational band and the 2721.1-keV state. This 41-keV transition has a measured γ-ray intensity 13(8) times smaller than the 323-keV transition in the projection of a sum of double gates between the 359-keV and 348-, 328-, 375-, and 910-keV transitions. The difference between these γ-ray intensities indicates a conversion coefficient of $\alpha_{\mathrm{tot}} = 12(8)$ for the 41-keV transition, which is consistent with $M1$ multipolarity. This evidence suggests a spin and parity of $I^\pi = \frac{21}{2}^+$ for the $E_x = 2721.1$ keV state. Intensity-balance measurements of this kind were used to infer other transition multipolarities, as summarized in Table II.

γ-γ angular correlation measurements were performed for pairs of transitions to gain an independent spin-parity/assessment of the $E_x = 2721.1$ keV state. Figure 3 presents angular correlation measurements for a selection of transition pairs in ^{121}Sb, also summarized in Table III. Data are fitted using Eq. (1). These measurements are based on the $E2$, 1145-keV transition [20] as a primary gate; they are also consistent with the $M1+E2$, 998-keV γ-ray mixing ratio published in Ref. [20]. The spins and parities of the states

TABLE II. Experimental internal conversion coefficient measurements, α_{tot}, compared with calculated values for transitions, γ_1, of energy $E_{\gamma 1}$.

Nucleus	$E_{\gamma 1}$ (keV)	Gate	$E_{\gamma 2}, E_{\gamma 3}\ldots$ (keV)	α_{tot} (exp.)	α_{tot} (the.) [22]					Assignment (E_{γ_1})
					$E1$	$M1$	$E2$	$M2$	$E3$	
^{121}Sb	41	{359}{348, 328, 375, 910}	323($M1$)	12(8)	2	8	43	198	2140	$M1(+E2)$
		{910, 375, 328, 348}	323($M1$),682($E2$)	15(3)						$M1+E2$
		{910, 375, 328, 348}	323($M1$),682($E2$)	15(3)						
	78	{359}{287}	348($M1$)	0.2(4)	0.4	1.3	4.2	17.1	62.5	$E1$
	85	{292}{1022}	998($M1$)	0.1(3)	0.3	1.0	3.0	11.8	40.3	$E1$
	117	{170}{998, 715, 391}	292($E2$)	0.47(17)	0.12	0.41	0.95	3.60	8.48	$M1$
	170	{117}{998, 715, 391}	292($E2$)	0.08(12)	0.04	0.14	0.26	0.94	1.54	$E1$ or $M1$
	287	{998}{391}	292($E2$)	0.02(5)	0.01	0.04	0.04	0.16	0.17	$E1$, $M1$, or $E2$
^{123}Sb	128	{1089}{956}	442($E2$)	0.85(15)	0.10	0.32	0.71	2.59	5.57	$E2$
		{1089}{442}	956($E2$)	0.75(14)						$E2$
		{956}{442}	1089($E2$)	0.69(13)						$E2$

on the right side of Fig. 1 are assigned on the basis of γ-γ angular correlations and intensity-balance measurements. The angular correlation measurements provide additional evidence for the $I^\pi = \frac{21}{2}^+$ spin parity of the $E_x = 2721.1$ keV state.

It is unlikely that the $E_x = 2721.1$ keV level is the origin of the long, $T_{1/2} = 200$ μs half-life. The Weisskopf single-particle transition rates for the 287- and 41-keV γ-ray decays, from an isomeric state with $T_{1/2} = 200\,\mu$s, are $B(E1) = 3.5 \times 10^{-11}$ and $B(M1) = 6.8 \times 10^{-8}$ W.u., respectively. These are inconsistent with transition rates observed systematically [21] by at least four orders of magnitude. It follows that to account for the isomeric half-life another level must exist that decays to the $E_x = 2721.1$ keV state via an unobserved, low-energy, highly converted transition, expressed by Δ in Fig. 1. By considering typical Weisskopf transition rates [21], the efficiency of Gammasphere, and the magnitude of the internal conversion process, the energy and multipolarity of Δ can be restricted to $E_\Delta(E2) < 60$ keV or $E_\Delta(M2) < 80$ keV. Based on these limitations, the $E_x = 2721.1 + \Delta$ keV state is tentatively assigned spin $I = (\frac{25}{2})$.

A number of previously unobserved γ rays, shown in Fig. 2(c), reveal the existence of a state at $E_x = 2057.1$ keV. The 85-keV transition is in coincidence with 1022-, 918-, and 913-keV γ rays, which decay to the $E_x = 1035.5$, 1139.4, and 1144.6 keV states, respectively. Intensity-balance measurements, summarized in Table II, indicate $E1$ multipolarity for the 85-keV γ ray; the $E_x = 2057$ keV level is assigned a spin parity of $I^\pi = \frac{13}{2}^+$.

A state with energy $E_x = 2551.2$ keV is inferred from the observation of 117- and 170-keV γ rays [see spectra in Figs. 2(d) and 2(e)]. The tentative 409-keV transition to the $E_x = 2142.0$ keV level, illustrated in Fig. 2(e), suggests the ordering of the 117- and 170-keV γ rays. Using intensity-balance arguments, summarized in Table II, the 117- and 170-keV γ rays are provided with $M1$ and $M1$ or $E1$ multipolarity, respectively. This information indicates a spin parity of $I^\pi = (\frac{21}{2}^-)$ or $(\frac{19}{2}^-)$ for the $E_x = 2551.2$ keV state.

A 401-keV γ ray has been observed in coincidence with the 170-keV transition and in anticoincidence with the 117-, 292-, and 287-keV lines. The spectrum in Fig. 2(e) shows coincidences among the 401-keV and 170-, 391-, 715-, and

TABLE III. Angular correlations for pairs of transitions γ_1 and γ_2 with mixing ratios δ_1 and δ_2, respectively. A_{22} and A_{44} coefficients are calculated using the prescription of Ref. [19]. These calculated values are compared with experimental ones obtained from data fitted to Eq. (1).

Nucleus	Initial state	γ_2 (keV)	$J_i^\pi \rightarrow J_f^\pi$	δ_2	γ_1 (keV)	Assignment (γ_1)	A_{22}	A_{44}	δ_1
^{121}Sb	$11/2^-$	1145	$9/2^+ \rightarrow 5/2^+$	0	282	$11/2^- \rightarrow 9/2^+$	−0.08(5)	−0.01(7)	$0.01^{+0.19}_{-0.14}$
	$15/2^-$	391	$11/2^- \rightarrow 9/2^+$	0	715	$15/2^- \rightarrow 11/2^-$	−0.12(3)	0.02(4)	$-0.17^{+0.19}_{-0.08}$
	$19/2^-$	715	$15/2^- \rightarrow 11/2^-$	0	292	$19/2^- \rightarrow 15/2^-$	0.097(19)	0.05(3)	$0.02^{+0.09}_{-0.07}$
	$21/2^+$	1145	$9/2^+ \rightarrow 5/2^+$	0	287	$21/2^+ \rightarrow 19/2^-$	−0.11(5)	−0.04(7)	0.03(14)
		715	$15/2^- \rightarrow 11/2^-$	0			−0.048(19)	0.01(3)	−0.04(6)
		292	$19/2^- \rightarrow 15/2^-$	0			−0.099(13)	0.03(2)	0.05(4)
^{123}Sb	$15/2^+$	1089	$11/2^+ \rightarrow 7/2^+$	0	956	$15/2^+ \rightarrow 11/2^+$	0.15(4)	0.00(6)	$-0.10^{+0.17}_{-0.25}$
	$19/2^+$	1089	$11/2^+ \rightarrow 7/2^+$	0	442	$19/2^+ \rightarrow 15/2^+$	0.13(4)	−0.07(6)	$-0.08^{+0.14}_{-0.18}$
	$23/2^+$	1089	$11/2^+ \rightarrow 7/2^+$	0	128	$23/2^+ \rightarrow 19/2^+$	0.14(5)	−0.00(6)	$-0.06^{+0.18}_{-0.21}$

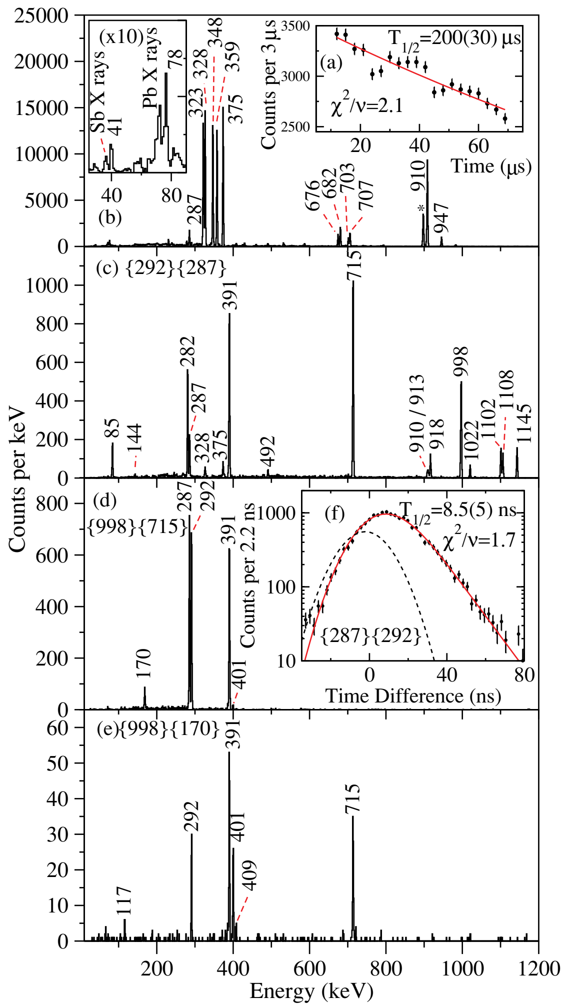

FIG. 2. (Color online) Panel (a) gives the time evolution of the $T_{1/2} = 200(30)$ μs isomer in ^{121}Sb, measured using summed double coincidence gates on all transitions. Panels (b)–(e) provide double-gated spectra; gates are given in parenthesis ($\{x\}\{y\}$) for each, except panel (b), which is a sum of double gates on all transitions in the rotational sequence of Fig. 1. Panel (f) illustrates the γ-ray time difference between the 287- and 292-keV transitions; the half-life is measured to be $T_{1/2} = 8.5(5)$ ns using a folded Gaussian plus exponential fit. The dashed line is the prompt Gaussian used in the fit [FWHM = 30(3) ns]. Contaminants from ^{204}Pb are indicated by asterisks (*). See text for further details.

998-keV transitions. The coincidence between the 401- and 715-keV γ rays implies that the 401-keV transition should be placed between the $E_x = 2551.2$ and 2142.0 keV levels. However, the energy of the γ ray does not match the difference between the states; a discrepancy of 8.3 keV remains. This provides evidence for another state at an energy of either $E_x = 2542.9$ or 2150.3 keV. Because it is less likely that an 8.3-keV transition of any multipolarity would compete with the 117- or 409-keV transitions (from the $E_x = 2542.9$ keV state), a tentative state of energy, $E_x = 2150.3$ keV is, therefore, assigned to ^{121}Sb.

In addition to the microsecond isomer, the $E_x = 2434.3$ keV, $I^\pi = \frac{19}{2}^-$ state was observed to be isomeric. Figure 2(f) provides the time difference between 287- and 292-keV γ rays. A folded Gaussian plus exponential fit of these data indicates a half-life of $T_{1/2} = 8.5(5)$ ns. The transition strengths for the 78-keV ($E1$) and 292-keV ($E2$) transitions are $B(E1) = (4.1 \pm 0.9) \times 10^{-6}$ and $B(E2) = 0.78(10)$ W.u., respectively. These are comparable with the transition strengths of the $E1$ and $E2\gamma$ rays decaying from the $I^\pi = \frac{19}{2}^-$, $E_x = 2553.6$ keV state in ^{119}Sb ($B(E1) = 7.3 \times 10^{-7}$ and $B(E2) = 0.026$ W.u., respectively [23]).

B. ^{123}Sb

The decay of two isomers has been observed for the first time. γ rays from the decay of states in ^{123}Sb were identified in projections of double coincidence gates placed on γ rays first reported in Ref. [11]. Figure 4 illustrates the partial level scheme of ^{123}Sb from the present experiments; Table IV provides a summary of all transitions observed.

1. $I = (27/2)\hbar$ isomer

The double-gated coincidence spectrum in the top panel of Fig. 5(a) shows the 1089-, 956-, 442-, and 128-keV transitions observed from the decay of a microsecond isomer. Figure 5(b) provides a time spectrum of transitions from the isomeric decay in the long-pulsing experiment; the half-life is measured to be $T_{1/2} = 52(3)$ μs.

Intensity-balance measurements (summarized in Table II) were performed for the 128-keV transition, providing strong evidence for $E2$ multipolarity. γ-γ angular correlation measurements between the 1089-keV and 956-, 442-, and 128-keV transitions are presented in Fig. 6 and summarized in Table III. The correlation between the 1089- and 128-keV transitions indicated either pure quadrupole (probably $E2$) or mixed dipole/quadrupole (probably $M1/E2$) character for the 1089-keV γ ray, which is consistent with the evaluation in Ref. [24]. Angular correlations summarized in Table III indicate pure quadrupole or mixed dipole/quadrupole character for the 442- and 956-keV transitions. In addition to angular correlation measurements, the nonobservation of transitions linking the $E_x = 2044.4$, 2486.3, and 2614.1 keV states to the (negative-parity) states on the left side of Fig. 4, indicated differences in angular momenta of $\Delta I \geqslant 2$. On the basis of these arguments, the $E_x = 1088.6$, 2044.4, 2486.3, and 2614.1 keV states are assigned spins and parities of $I^\pi = \frac{11}{2}^+$, $\frac{15}{2}^+$, $\frac{19}{2}^+$, and $\frac{23}{2}^+$, respectively.

The $T_{1/2} = 52(3)$ μs half-life appears to derive from the $E_x = 2614.1$ keV level, decaying via the 128-keV transition. This corresponds to a single-particle transition rate of $B(E2) = 5.3(1) \times 10^{-3}$ W.u. This is approximately 5 times smaller than that of the $I^\pi = \frac{21}{2}^-$ state in ^{121}Sb and 10 times smaller than the $I^\pi = \frac{21}{2}^-$ state in ^{119}Sb [12]. In regard to the discrepancy in transition strength, it is noted that the $T_{1/2} = 52$ μs half-life may derive from a state higher in energy than the $E_x = 2614.0$ keV level, decaying via an unobserved, low-energy, highly converted transition.

TABLE IV. A summary of γ-ray energies, E_γ in ^{123}Sb between states with spin and parity, J_i^π and J_f^π, and energy, E_i and E_f. γ-ray intensities for transitions on the right and left side of Fig. 4 are given by I_γ(R) and I_γ(L) from the long-pulsing and short-pulsing experiments, respectively.

E_γ (keV)	E_i (keV)	E_f (keV)	J_i^π	J_f^π	I_γ(R)	I_γ(L)
127.8(3)	2614.1	2486.3	$23/2^+$	$19/2^+$	60(5)	–
160.3(5)	160.1	0.0	$5/2^+$	$7/2^+$	–	25(3)
201.0(4)	2239.1	2038.2	$(19/2^-)$	$(15/2^-)$	–	104(18)
381.7(4)	2038.2	1656.5	$(15/2^-)$	$(11/2^-)$	–	114(15)
396.0(5)	1656.5	1260.7	$(11/2^-)$	$9/2^+$	–	29(3)
441.9(3)	2486.3	2044.3	$19/2^+$	$15/2^+$	109(11)	–
567.7(4)	1656.5	1088.6	$(11/2^-)$	$11/2^+$	–	14(3)
626.1(4)	1656.5	1030.3	$(11/2^-)$	$9/2^+$	–	94(7)
955.8(3)	2044.3	1088.6	$15/2^+$	$11/2^+$	112(9)	–
1030.3(4)	1030.3	0.0	$9/2^+$	$7/2^+$	–	100(8)
1088.6(3)	1088.6	0.0	$11/2^+$	$7/2^+$	100	–
1100.9(5)	1260.7	160.1	$9/2^+$	$5/2^+$	–	18(4)
1260.9(7)	1260.7	0.0	$9/2^+$	$7/2^+$	–	7(2)

2. $I^\pi = (19/2^-)$ and $(15/2^-)$ isomers

Transitions from the decay of the $E_x = 2239.1$ keV isomeric state (initially reported in Ref. [11] with $T_{1/2} = 110(10)$ ns) were observed in the short-pulsing experiment. The double-gated coincidence spectra in Figs. 5(c) and 5(d) show γ-ray decays from this isomer, which are summarized in Table IV. Figure 5(e) illustrates a time spectrum, double gated on delayed transitions from the isomeric $E_x = 2239.1$ keV level; relative to the accelerator RF signal, the half-life of the decay is measured as $T_{1/2} = 190(30)$ ns. With regard to the large discrepancy between the value observed in this work and that presented in Ref. [11], timing calibration was extensively checked with the accurate measurement of other, previously observed, isomeric states.

The $E_x = 2038.1$ keV state was also observed to be isomeric; Fig. 5(f) provides a time difference spectrum between the 201-keV transition, and those from the decay of states below the isomer. The half-life of the state was measured to be $T_{1/2} = 37(4)$ ns using a folded Gaussian plus exponential fit.

Due to insufficient statistics, it was not possible to assign spins and parities to the states populated from the decay of the $T_{1/2} = 190$ ns isomer, using angular correlations. Tentative spins and parities are, therefore, adopted from the systematic arguments proposed in Ref. [11].

Transition strengths for the 201- and 382-keV γ rays are $B(E2) = 0.22(2)$ and 0.048(2) W.u., respectively, which are consistent with those of other $E2$ transitions observed locally [12,25].

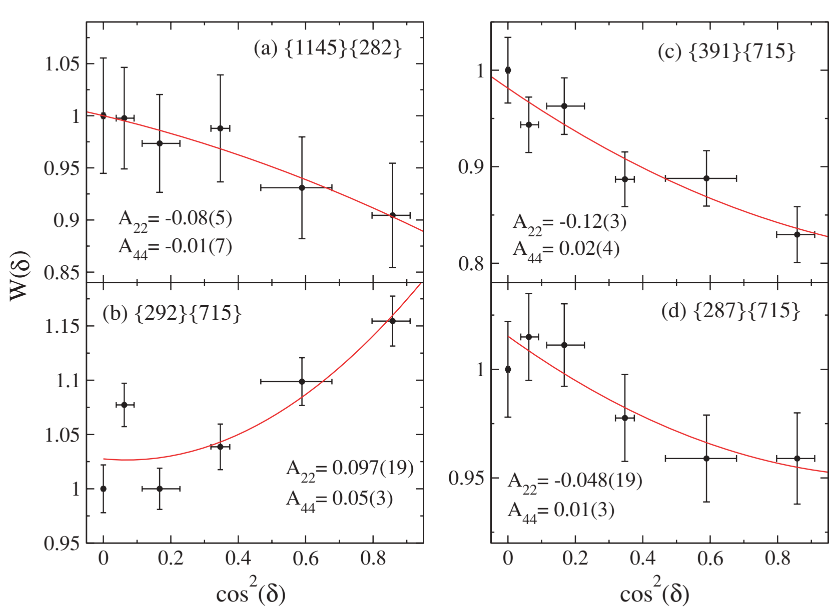

FIG. 3. (Color online) Representative angular correlation measurements for transitions in ^{121}Sb. Information on the γ-γ coincidences (E_x, E_y) involved is provided in each case by $\{x\}\{y\}$.

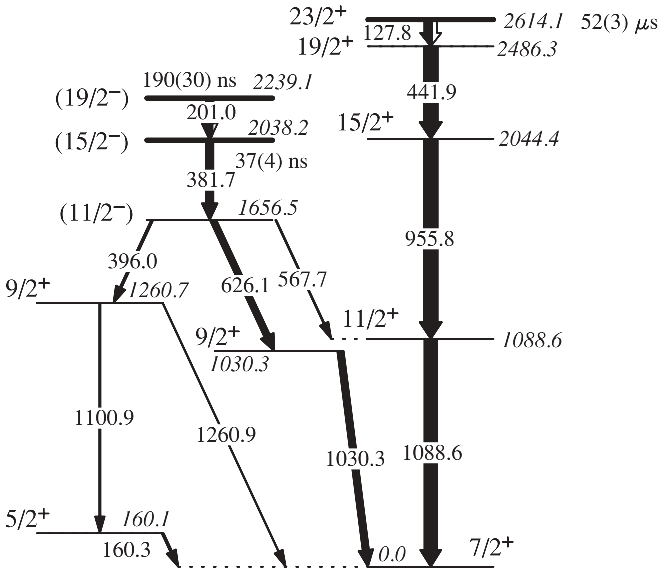

FIG. 4. Level scheme for transitions in ^{123}Sb observed in this experiment from the decay of $T_{1/2} = 190(30)$ ns and 52(3) μs isomers.

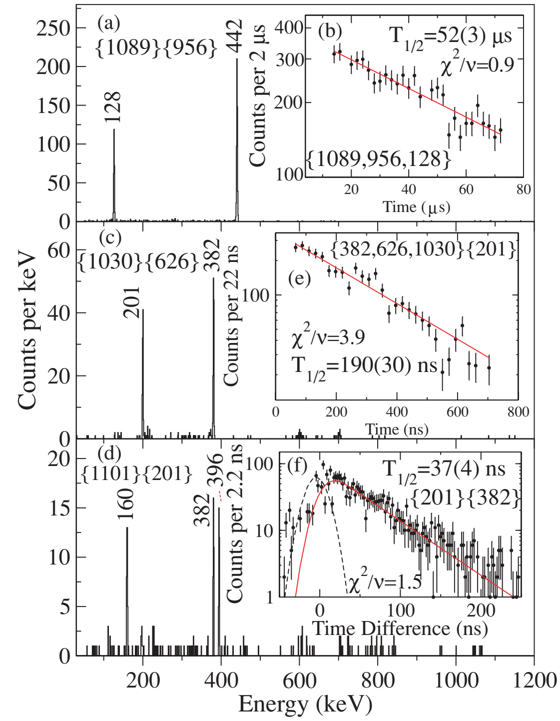

FIG. 5. (Color online) The spectrum in panel (a) illustrates γ rays from the decay of a microsecond isomer in ^{123}Sb. The time evolution of its decay is given in spectrum (b). From double gates on all transitions from its decay, the half-life is measured to be $T_{1/2} = 52(3)$ μs. Double-gated spectra in panels (c) and (d) show γ rays from the decay of an isomer identified in the short-pulsing experiment. The time evolution of its decay is provided in panel (e); the half-life is measured to be $T_{1/2} = 190(30)$ ns using a folded Gaussian plus exponential fit. Spectrum (f) illustrates the γ-ray time difference between the 201-keV transition and those from the decay of states below the isomeric $E_x = 2038.2$ keV state; the half-life is measured to be $T_{1/2} = 37(4)$ ns using a folded Gaussian plus exponential fit. The dashed line is the prompt Gaussian used in the fit [FWHM = 30(3) ns]. Gates for each spectrum are provided in parenthesis ($\{x\}\{y\}$).

V. DISCUSSION

When the levels schemes for ^{121,123}Sb are compared (Figs. 1 and 4, respectively), one observes a number of differences in the distribution and decay of nuclear states. This is due to a combination of the change in quantum number for the respective ground states between ^{121}Sb and ^{123}Sb and the fact that the rotational band built on the $\pi\frac{9}{2}[404]$ intruder state (observed in $^{113-121}$Sb [5–8]) becomes nonyrast in odd-A antimony nuclei with $123 \leqslant A \leqslant 131$. Despite these differences, the multiparticle level structure of these nuclei is well described by considering neutron states in neighboring tin nuclei coupled to the extra proton [11,12].

Figure 7 illustrates a systematic correlation between the yrast states in ^{121,123}Sb and their tin isotones, ^{120,122}Sn. The $I^\pi = 10^+$ state, present in even-tin nuclei from $116 \leqslant A \leqslant 130$, is interpreted as a pure $\nu(h_{\frac{11}{2}})^2$ excitation [12,25]. Similarly, the $I^\pi = \frac{25}{2}^+$ levels in ^{117,119}Sb are associated with a $d_{\frac{5}{2}}$ proton maximally aligned to the $I^\pi = 10^+$ states in the neighboring isotones ^{116,118}Sn [12]. The $I^\pi = (\frac{25}{2}^+)$ spin parity of the isomeric state in ^{121}Sb is systematically consistent with the spin of the isomeric states in ^{117,119}Sb. As such, the configuration of the isomer is adopted tentatively as $\pi d_{\frac{5}{2}} \otimes \nu(h_{\frac{11}{2}})^2$. However, it is noted that because the energy between the $d_{\frac{5}{2}}$ and $g_{\frac{7}{2}}$ proton orbitals is so small ($\sim$50 keV [1]), there is likely to be a significant $\pi g_{\frac{7}{2}}$ admixture in the wave function of these states.

It is important to note a limitation with this assessment, based on energy/spin systematics in nearby Sn isotones, because there are large discrepancies between the transition rates in these nuclei: the 197-keV transition in ^{120}Sn (from the $I^\pi = 7^-$ state) is approximately 200 times faster than the analog $E2$ transition in ^{121}Sb (from the $I^\pi = \frac{19}{2}^-$ state), whereas the 163-keV transition in ^{122}Sn (from the $I^\pi = 7^-$ state) is approximately 15 times faster than the 201-keV transition [from the $I^\pi = (\frac{19}{2}^-)$ state] in ^{123}Sb. On the basis of the current data we are unable to identify the physical origin of such differences; the discrepancies may reflect significant differences in wave function between these states. Given the paucity of an exact theoretical description for these states, such as that provided by shell-model calculations with a physical model space, such assignments should be made with caution. Nevertheless, the correlation between the energies/spins of states in neighboring Sn and Sb nuclei is striking, for which, in the absence of such theoretical examination, it may seem sensible to draw these comparisons.

Shell-model calculations have been performed for ^{127,129,131}Sb and ^{126,128,130}Sn using the model space and Hamiltonian described in Ref. [26], with the shell-model codes OXBASH [27] and ANTOINE [28]. It was not possible to perform calculations for lighter antimony nuclides without severely truncating the model space. Experimental level energies are well reproduced by shell-model calculations, in most cases

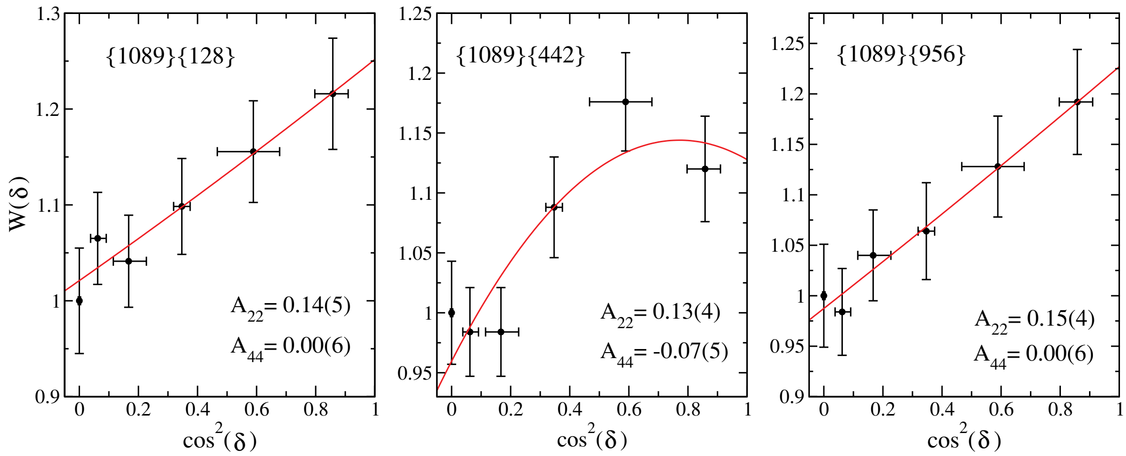

FIG. 6. (Color online) Representative angular correlation measurements for transitions in ^{123}Sb. Information on the γ-γ coincidences (E_x, E_y) involved is provided in each case by $\{x\}\{y\}$.

to within 200 keV. Figure 8 provides a comparison between empirical and calculated energies for the first-excited $I^\pi = \frac{23}{2}^+$, $\frac{19}{2}^-$, and $\frac{15}{2}^-$ states. A noteworthy feature of this plot is the indication of a $I^\pi = \frac{23}{2}^+$ level in ^{127}Sb that has not been observed experimentally, due probably to the paucity of spectroscopic data for this neutron-rich nucleus. The $I^\pi = \frac{23}{2}^+$ isomer in ^{123}Sb is interpreted as the isotopic analog of the states in ^{127,129,131}Sb. The orbital occupation numbers for each of these calculated states is provided in Table V; a leading $\pi g_{\frac{7}{2}} \otimes \nu(h_{\frac{11}{2}})^{-2}$ configuration is associated with the $I^\pi = \frac{23}{2}^+$ states.

The configurations of the 5^- and 7^- levels in even-A tin nuclei involve a neutron in the intruder $h_{\frac{11}{2}}$ orbital, coupled to an even-parity orbital from the $N = 4$ harmonic oscillator shell, with leading neutron configurations of $\nu(h_{11/2} \otimes d_{3/2})$ and $\nu(h_{11/2} \otimes s_{1/2})$, respectively [29]. The $I^\pi = \frac{15}{2}^-$ and

TABLE V. Wave function occupation numbers taken from shell-model calculations discussed in the text.

Nucleus	I^π	$\nu d_{\frac{5}{2}}$	$\nu g_{\frac{7}{2}}$	$\nu d_{\frac{3}{2}}$	$\nu s_{\frac{1}{2}}$	$\nu h_{\frac{11}{2}}$	$\pi g_{\frac{7}{2}}$	$\pi d_{\frac{5}{2}}$
^{130}Sn	10^+	8.00	6.00	4.00	2.00	10.00		
	7^-	7.99	5.99	3.02	2.00	11.00		
	5^-	7.99	5.98	3.42	1.60	11.00		
^{131}Sb	$\frac{23}{2}^+$	8.00	6.00	4.00	2.00	10.00	0.98	0.01
	$\frac{19}{2}^-$	7.98	5.98	3.05	2.00	11.00	0.99	0.01
	$\frac{15}{2}^-$	7.99	5.99	3.19	1.84	11.00	0.99	0.00
^{128}Sn	10^+	7.87	5.83	3.05	1.74	9.51		
	7^-	7.87	5.83	2.79	1.76	9.76		
	5^-	7.87	5.80	2.85	1.50	9.99		
^{129}Sb	$\frac{23}{2}^+$	7.87	5.82	2.86	1.67	9.78	0.98	0.01
	$\frac{19}{2}^-$	7.85	5.80	2.68	1.64	10.04	0.98	0.01
	$\frac{15}{2}^-$	7.85	5.77	2.59	1.36	10.43	0.98	0.01
^{126}Sn	10^+	7.72	5.66	2.59	1.53	8.50		
	7^-	7.71	5.66	2.40	1.48	8.75		
	5^-	7.71	5.63	2.39	1.32	8.96		
^{127}Sb	$\frac{23}{2}^+$	7.69	5.62	2.47	1.43	8.80	0.98	0.01
	$\frac{19}{2}^-$	7.68	5.63	2.22	1.39	9.08	0.98	0.01
	$\frac{15}{2}^-$	7.69	5.61	2.29	1.18	9.23	0.97	0.01

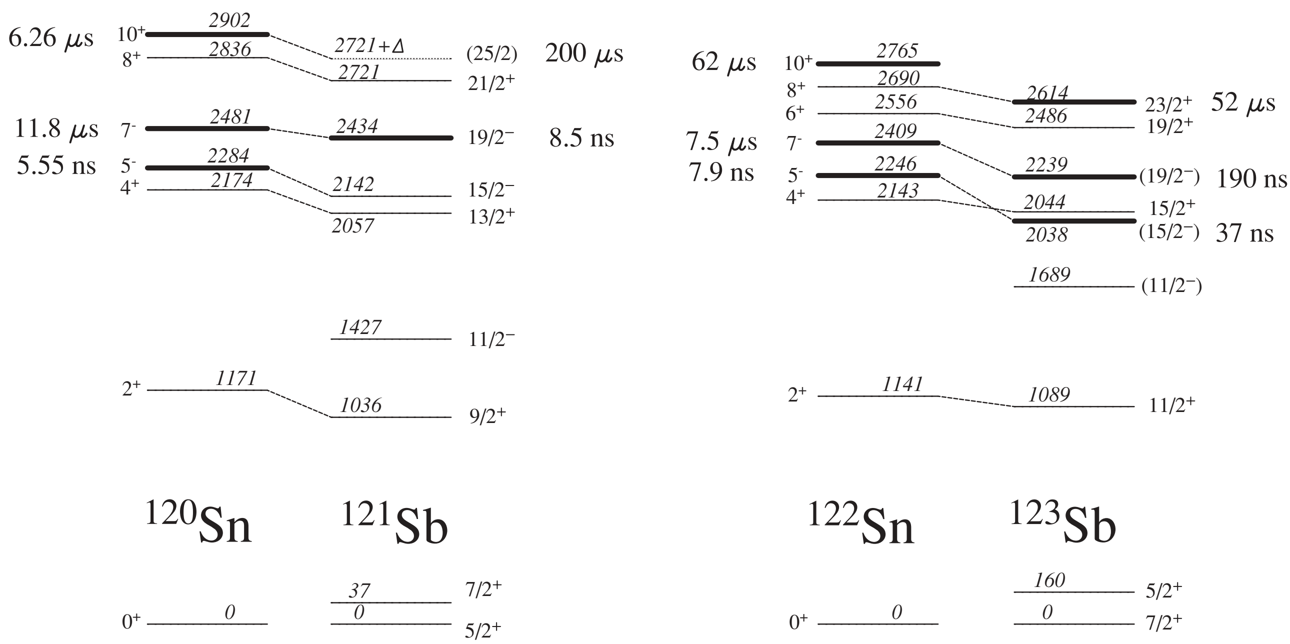

FIG. 7. Comparison of states in ^{121,123}Sb with those in isotonic tin neighbors, ^{120,122}Sn. Levels connected with dashed lines are interpreted as states with the same leading neutron configurations.

$\frac{17}{2}^-$ states in odd antimony nuclei with $113 \leqslant A \leqslant 131$ are associated with these configurations, coupled to a $d_{\frac{5}{2}}$ or $g_{\frac{7}{2}}$ proton [11,12]. Orbital occupation numbers from shell-model calculations (provided in Table V) are consistent with the configuration assignments for these states.

The top panel of Fig. 9 shows the energy of the $I^\pi = 5^-$ and 7^- states in even-A tin nuclei with increasing neutron excess, in comparison to the $I^\pi = \frac{15}{2}^-$ and $\frac{19}{2}^-$ in odd-A antimony nuclei. One can see that the excitation energy of these states steadily decreases with the addition of neutrons. There also appears to be a bifurcation of the antimony and tin state energies, with the antimony states becoming more bound with increasing neutron excess, relative to the corresponding tin states. The bottom panel of Fig. 9 plots the difference in energy between negative-parity states in antimony and tin

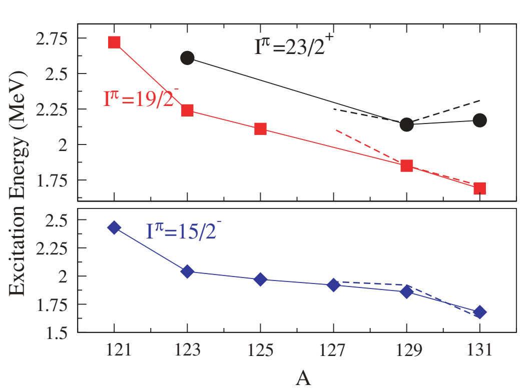

FIG. 8. (Color online) Energy of states from shell-model calculations (dashed lines) compared with those observed empirically from this work and Refs. [12,30,31].

with the same neutron configuration. A noteworthy feature of this picture is the asymptotic behavior of both plots, which

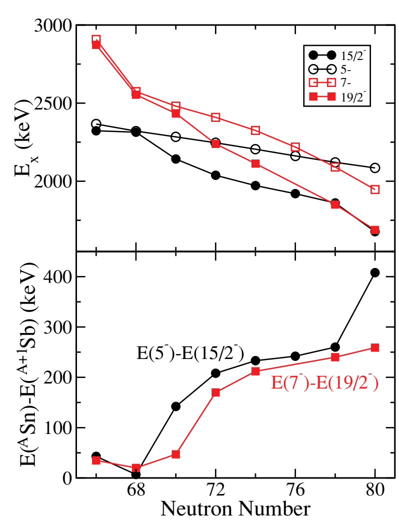

FIG. 9. (Color online) The top panel illustrates the evolution of negative-parity states in antimony and tin nuclei with $N = 66$–80 taken from Refs. [12,30,31]. Open square symbols (red) represent $I^\pi = 7^-$ states in tin nuclei, whereas filled squares (red) show $\frac{19}{2}^-$ states in antimony. Open circle symbols (black) represent $I^\pi = 7^-$ states in tin nuclei, whereas filled circles (black) show $\frac{19}{2}^-$ states in antimony. The bottom panel provides the energy difference between these states; the square symbols (red) show the energy difference between the $I^\pi = 7^-$ (Sn) and $\frac{19}{2}^-$ (Sb) states, whereas circles (black) illustrate the difference between the $I^\pi = 5^-$ (Sn) and $\frac{15}{2}^-$ (Sb) levels.

approach a limit of ~250 keV (excluding the $N = 80$ data point for the $\frac{15}{2}^-/5^-$ energy difference).

The difference in energy between the tin and antimony negative-parity states must derive from the addition of the additional proton, i.e., from the neutron-proton residual interaction. According to Fig. 9, the $I^\pi = \frac{15}{2}^-$ and $\frac{19}{2}^-$ states in odd-antimony nuclei are lowered by up to $E \sim 250$ keV. The occupation numbers for the wave functions of the $I^\pi = \frac{15}{2}^-$ and $\frac{19}{2}^-$ levels in ^{127,129,131}Sb, from Table V, illustrate the dominance of the $\pi g_{\frac{7}{2}}$ orbital. The monopole energy shift of the $\pi g_{\frac{7}{2}}$ level has been interpreted as a signature of a strong tensor force between the $h_{\frac{11}{2}}$ neutron and $g_{\frac{7}{2}}$ proton orbitals with increasing neutron excess in the $\nu h_{\frac{11}{2}}$ subshell [4]. The systematic (~250 keV) energy difference between states in tin and antimony, illustrated in the bottom panel of Fig. 9, is interpreted here as the manifestation of this residual interaction between the $g_{\frac{7}{2}}$ proton and $h_{\frac{11}{2}}$ neutron. In Fig. 9 the energy difference is reduced to almost zero as neutron number approaches $N = 68$, the inversion point of the $g_{\frac{7}{2}}$ and $d_{\frac{5}{2}}$ protons. At this point, the $d_{\frac{5}{2}}$ proton would be expected to have a significant contribution to the wave function of the $I^\pi = \frac{15}{2}^-$ and $\frac{19}{2}^-$ states. The energy difference here thus illustrates a reduction in the residual interaction between the $\nu h_{\frac{11}{2}}$ and $\pi d_{\frac{5}{2}}$ particles indicated in Ref. [4].

VI. SUMMARY

In conclusion, high-spin states have been identified in the stable nuclei, ^{121,123}Sb following fusion-fission reactions between ^{178}Hf and ^{27}Al. Multidimensional γ-ray coincidence techniques have been used to identify a number of previously unreported states, including four isomers. Angular correlation measurements have been used with intensity-balance techniques to identify spins and parities of states in these nuclei. The states observed in these nuclei are interpreted as multiparticle states formed from the coupling of a $d_{\frac{5}{2}}$ or $g_{\frac{7}{2}}$ proton with $\nu h_{\frac{11}{2}}$, $\nu s_{\frac{1}{2}}$, and $\nu d_{\frac{3}{2}}$ excitations, observed in neighboring tin nuclei.

The energies of negative-parity states have been compared in tin and antimony nuclei. The difference in these energies has been interpreted as the manifestation of the proton-neutron residual interaction, recently associated with a strong tensor force.

Shell-model calculations have been performed for ^{126,128,130}Sn and ^{127,129,131}Sb. The calculated excitation energies of states in these nuclei compare favorably with those observed empirically and predict the existence of a low-lying $I^\pi = \frac{23}{2}^+$ state in ^{127}Sb. Using systematic arguments, a $I^\pi = \frac{23}{2}^+$ state is also expected in ^{125}Sb, as the isotopic analog of $I^\pi = \frac{23}{2}^+$ states in odd-A antimony nuclei from $123 \leqslant A \leqslant 131$.

Shell-model calculations provide an accurate description for excited states around the "doubly magic" ^{132}Sn core. However, as the number of valence particles/holes increases, the resources required to perform such calculations increases exponentially. The spectroscopic results obtained in this work have contributed to the data available for $Z = 51$ nuclei between stability and the closed-shell at $N = 82$ and provide an empirical benchmark for which to test the development of these theoretical descriptions.

ACKNOWLEDGMENTS

The author acknowledges helpful discussions with R. Orlandi, B. A. Brown, and P. H. Regan. This work is supported by the US Department of Energy, Office of Nuclear Physics, under contract number DE-AC02-06CH11357 (ANL); US AFOSR under contract number F49620-02-1-0187; the AWE (UK); and the EPSRC (UK).

[1] M.-G. Porquet, S. Peru, and M. Girod, Eur. Phys. J. A **25**, 319 (2005).
[2] J. P. Schiffer, S. J. Freeman, J. A. Caggiano, C. Deibel, A. Heinz, C.-L. Jiang, R. Lewis, A. Parikh, P. D. Parker, K. E. Rehm, S. Sinha, and J. S. Thomas, Phys. Rev. Lett. **92**, 162501 (2004).
[3] R. B. Firestone and V. S. Shirley, *Table of Isotopes*, 8th ed. (Wiley, New York, 1996).
[4] T. Otsuka, T. Matsuo, and D. Abe, Phys. Rev. Lett. **97**, 162501 (2006).
[5] D. R. LaFosse, D. B. Fossan, J. R. Hughes, Y. Liang, H. Schnare, P. Vaska, M. P. Waring, and J.-Y. Zhang, Phys. Rev. C **56**, 760 (1997).
[6] C.-B. Moon, C. S. Lee, J. C. Kim, J. H. Ha, T. Komatsubara, T. Shizuma, K. Uchiyama, K. Matsuura, M. Murasaki, Y. Sasaki, H. Takahashi, Y. Tokita, and K. Furuno, Phys. Rev. C **58**, 1833 (1998).
[7] R. S. Chakrawarthy and R. G. Pillay, Phys. Rev. C **54**, 2319 (1996).
[8] W. F. Piel, Jr., P. Chowdhury, U. Garg, M. A. Quader, P. M. Stwertka, S. Vajda, and D. B. Fossan, Phys. Rev. C **31**, 456 (1985).
[9] M. Conjeaud, S. Harar, M. Caballero, and N. Cindro, Nucl. Phys. **A215**, 383 (1973).
[10] K. Heyde, Phys. Rep. **102**, 291 (1983).
[11] M.-G. Porquet, Ts. Venkova, R. Lucas, A. Astier, A. Bauchet, I. Deloncle, A. Prevost, F. Azaiez, G. Barreau, A. Bogachev, N. Buforn, A. Buta, D. Curien, T. P. Doan, L. Donadille, O. Dorvaux, G. Duchene, J. Durell, Th. Ethvignot, B. P. J. Gall, D. Grimwood, M. Houry, F. Khalfallah, W. Korten, S. Lalkovski, Y. Le Coz, M. Meyer, A. Minkova, I. Piqueras, N. Redon, A. Roach, M. Rousseau, N. Schulz, A. G. Smith, O. Stezowski, Ch. Theisen, and B. J. Varley, Eur. Phys. J. A **24**, 39 (2005).
[12] S. Lunardi, P. J. Daly, F. Soramel, C. Signorini, B. Fornal, G. Fortuna, A. M. Stefanini, R. Broda, W. Meczynski, and J. Blomqvist, Z. Phys. A **328**, 487 (1987).
[13] G. A. Jones, Ph.D. thesis, University of Surrey, 2006.
[14] I-Y. Lee, Nucl. Phys. **A520**, 641c (1990).
[15] W. Urban *Ana Software* (private communication).
[16] D. Radford, Nucl. Instrum. Methods A **361**, 297 (1995).
[17] D. Radford, Nucl. Instrum. Methods A **361**, 306 (1995).
[18] B. Fornal, S. Zhu, R. V. F. Janssens, M. Honma, R. Broda, B. A. Brown, M. P. Carpenter, S. J. Freeman, N. Hammond,

F. G. Kondev, W. Krolas, T. Lauritsen, S. N. Liddick, C. J. Lister, S. Lunardi, P. F. Mantica, N. Marginean, T. Mizusaki, E. F. Moore, T. Otsuka, T. Pawlat, D. Seweryniak, B. E. Tomlin, C. A. Ur, I. Wiedenhover, and J. Wrzesinski, Phys. Rev. C **72**, 044315 (2005).
[19] G. D. Dracoulis, G. J. Lane, F. G. Kondev, A. P. Byrne, T. Kibedi, H. Watanabe, I. Ahmad, M. P. Carpenter, S. J. Freeman, R. V. F. Janssens, N. J. Hammond, T. Lauritsen, C. J. Lister, G. Mukherjee, D. Seweryniak, P. Chowdhury, and S. K. Tandel, Phys. Rev. C **71**, 044326 (2005).
[20] T. Tamura, Nucl. Data Sheets **90**, 107 (2000).
[21] P. Endt, At. Data Nucl. Data Tables **26**, 47 (1981).
[22] F. Rosel, H. M. Fries, K. Alder, and H. C. Pauli, At. Nucl. Data Tables **21**, 91 (1978).
[23] S. Ohya and K. Kitao, Nucl. Data Sheets **89**, 345 (2000).
[24] S. Ohya, Nucl. Data Sheets **102**, 547 (2004).
[25] R. Broda, R. H. Mayer, I. G. Bearden, Ph. Benet, P. J. Daly, Z. W. Grabowski, M. P. Carpenter, R. V. F. Janssens, T. L. Khoo, T. Lauritsen, E. F. Moore, S. Lunardi, and J. Blomqvist, Phys. Rev. Lett. **68**, 1671 (1992).
[26] B. A. Brown, N. J. Stone, J. R. Stone, I. S. Towner, and M. Hjorth-Jensen, Phys. Rev. C **71**, 044317 (2005); Erratum-*ibid.* **72**, 029901(E) (2005).
[27] B. A. Brown, A. Etchegoyen, N. S. Godwin, W. D. M. Rae, W. A. Richter, W. E. Ormand, E. K. Warburton, J. S. Winfield, L. Zhao, and C. H. Zimmerman, MSU-NSCL report number 1289 (2004).
[28] E. Caurier and E. Nowacki, Acta Phys. Pol. B **30**, 705 (1999).
[29] K. Krien, B. Klemme, R. Folle, and E. Bodenstedt, Nucl. Phys. **A228**, 15 (1974).
[30] J. A. Pinston and J. Genevey, J. Phys. G **30**, R57 (2004).
[31] D. S. Judson, A. M. Bruce, M. J. Taylor, G. D. Dracoulis, T. Kibedi, A. P. Byrne, K. H. Maier, P. Nieminen, and J. N. Orce, J. Phys. G **31**, S1899 (2005).